Available online at www.sciencedirect.com

SciVerse ScienceDirect

Ceramics International 39 (2013) 7425–7432

CERAMICS INTERNATIONAL

www.elsevier.com/locate/ceramint

Sol–gel derived undoped and boron-doped ZnO semiconductor thin films: Preparation and characterization

Chien-Yie Tsay*, Wei-Tse Hsu

Department of Materials Science and Engineering, Feng Chia University, Taichung 40724, Taiwan

Received 21 December 2012; received in revised form 21 February 2013; accepted 25 February 2013
Available online 7 March 2013

Abstract

We report the influence of boron doping concentration on the microstructure, electrical and optical properties of solution-processed zinc oxide (ZnO) thin films. The B doping concentration in the resultant solutions was varied from 0 to 5 at%, and the pH value of each synthetic solution was adjusted to 7.0. XRD measurements, SEM observations, and SPM examinations revealed that boron doping produced ZnO thin films consisting of a fine grain structure with a flat surface morphology. Moreover, ZnO thin films doped with B raised the texture coefficient along the (002) plane. All B-doped ZnO (ZnO:B) thin films exhibited higher transparency than that of the undoped ZnO thin film in the wavelengths between 350 and 650 nm. The optical band gap and Urbach energy of the ZnO:B thin films were higher than those of the undoped thin film. According to electrical transport characteristics, the 1% B-doped ZnO thin film exhibited the highest Hall mobility of 17.9 $cm^2/V\,s$, the highest electron concentration of $1.2\times10^{15}\,cm^{-3}$, and the lowest electrical resistivity of $2.2\times10^{2}\,\Omega\,cm$ among all of the ZnO:B thin films.

Keywords: A. Films; A. Sol–gel processes; C. Electrical properties; C. Optical properties; D. ZnO

1. Introduction

Polycrystalline ZnO-based thin films are widely used in numerous optoelectronic applications, such as surface acoustic wave devices, chemical sensors, optical detectors, photovoltaic devices, and field-effect transistors [1,2]. In the past decade, ZnO has been extensively studied because it is a non-toxic, chemically and thermally stable semiconductor, and its stability in hydrogen plasma is comparable to those of other transparent conductive oxide (TCO) materials [3,4]. Furthermore, ZnO-based thin films can be modified to have high conductivity, high transparency, high infrared reflectance, and enhanced electron mobility [5].

The electrical conductivity of pure ZnO is associated with deviation from stoichiometry due to the existence of native defects (oxygen vacancies and zinc interstitials). Further enhancement of the electrical properties of ZnO can be achieved by using dopants to substitute for zinc atoms, principally the group IIIA elements (e.g., B, Al, Ga, and In) [6–8]. In addition, it has been demonstrated that the electrical properties of impurity doped ZnO thin films are more stable than those of pure ZnO thin films, particularly those of films subjected to high temperature [9]. Among the group IIIA elements, boron possesses the lowest ionic radius (0.23 Å) and the highest electronegativity (2.04, Pauling). In addition, B^{3+} has a remarkably higher Lewis acid strength (10.7) than that of Al^{3+} (3.04) [9]. Therefore, boron doping could be effective for tuning the physical properties of ZnO thin films [10].

Recently, the use of boron-doped ZnO (ZnO:B) films as a TCO layer has attracted interest because such films exhibit stable electrical properties [11–13] and provide a promising potential for improving the conversion of thin-film solar cells [14–16]. Chen et al. reported the degradation effect with time of ZnO and ZnO:B films grown by metal-organic chemical vapor deposition (MOCVD) [11]. They demonstrated that the sheet resistance of ZnO:B films remained at a constant value after 30 days in air; however, that of ZnO films did not. Steinhauser et al. reported that heavily doped ZnO:B films deposited by low-pressure chemical vapor deposition (LPCVD) exhibited

*Corresponding author. Tel.: +886 4 24517250x5312; fax: +886 4 24510014.
E-mail address: cytsay@fcu.edu.tw (C.-Y. Tsay).

0272-8842/$ - see front matter © 2013 Elsevier Ltd and Techna Group S.r.l. All rights reserved.
http://dx.doi.org/10.1016/j.ceramint.2013.02.086

more stable resistivity after 800 h of damp heat treatment [12]. Shah et al. also reported that LPCVD ZnO:B films passed the standard damp heat test [13].

Various deposition techniques have been used to fabricate ZnO:B thin films, including chemical vapor deposition, magnetron sputtering, atomic layer deposition, pulse laser deposition, electrochemical deposition, spray pyrolysis, and the sol–gel method. Among these processes, the sol–gel method is a simple, non-vacuum deposition process that offers several advantages over vacuum deposition techniques, such as cost effectiveness, large area coating capability, and ease of compositional modification. Moreover, the sol–gel method may be combined with printing techniques (e.g., inkjet printing and micro-contact printing) to develop a maskless fabrication process for patterning of electrodes and active layers for optoelectronic devices [17–19].

The scientific and technical literatures on ZnO:B thin films focused primarily on developing a ZnO:B thin film with high conductivity and high transparency over the visible light spectrum. Such films are being considered as alternatives to conventional indium tin oxide (ITO) in thin-film transparent electrodes. Furthermore, impurity doped ZnO thin films have also been used as channel layers in high performance field-effect transistors (FETs) because they exhibit high electron mobility with a suitable electron concentration [20–22]. This study examined the effect of the incorporation of boron into ZnO semiconductor thin films on structural characteristics and investigated the influence of changes in microstructure and surface conditions on the electrical and optical properties of ZnO:B semiconductor thin films. In addition, we also discuss the major electron scattering mechanisms in the as-prepared transparent oxide semiconductor (TOS) thin films.

2. Experimental

The starting material, solvent, and stabilizer were zinc acetate dihydrate (ZnAc), 2-methoxyethanol (2-ME), and diethanolamine (DEA), respectively. Trimethyl borate (TMB) was chosen as the boron dopant source. The precursor solutions were synthesized by dissolving ZnAc and TMB in a mixture of 2-ME and DEA. The B doping concentration ([B]/[Zn+B]) in resultant solutions was varied from 0 to 5 at%. The molar ratio of sol stabilizer (DEA) and metal ions was maintained at 1.0 and the concentration of metal ions was kept at 0.5 M. Each solution was stirred using a magnet stirrer at 60 °C for 2 h to yield a clear and homogeneous solution, and then glacial acetic acid was added to adjust the pH value to 7.0. The resultant solutions were then aged for 72 h at room temperature before application as the coating solutions. Undoped and boron-doped ZnO (ZnO:B) sol–gel films were formed by spin coating the precursor solutions onto the pre-cleaned alkali-free glasses (NEG OA-10, dimensions: 50 mm × 50 mm × 0.7 mm) at 1000 rpm for 30 s. The cleaning procedures of glass substrates were described in detail in our previous report [23]. After spin coating, the sol–gel films were dried at 300 °C for 10 min to evaporate the solvent and remove organics. The procedures from spin coating and drying were repeated twice. Finally, these dried sol–gel films were annealed at 500 °C for 1 h under ambiance air to decompose the residual organics as well as to form the polycrystalline oxide films.

The crystallographic structures of the undoped and B-doped ZnO thin films were determined by X-ray diffractometer (Bruker D8 SSS) with CuKα radiation ($\lambda = 1.5406$ Å) at a glancing incident angle of 0.8 °. Plane-view and cross-sectional view micrographs of these thin films were acquired by a field-emission scanning electron microscope (FE-SEM, Hitachi S-4800). The film thickness of each thin film sample was evaluated from the corresponding cross-sectional FE-SEM image. The surface topography and roughness level were determined by tapping mode scanning probe microscopy (SPM, Digital Instrument NS4/D3100CL/MultiMode) with a scanning area of 0.5 μm × 0.5 μm. The electrical transport characteristics were measured by a Hall measurement system (Ecopia HMS-3000) using the van der Pauw configuration under 0.55 T magnetic field at room temperature. The optical transmittance of the glass/oxide thin film samples was examined by a UV–vis spectrophotometer (Hitachi U-2900) in the wavelength range of 200–800 nm.

3. Results and discussion

3.1. Analysis of structural and surface morphological properties of ZnO:B thin films

The pH value of a sol determines the microstructures of a sol–gel derived polycrystalline ZnO-based thin film, which in turn affects the electrical and optical properties [4]. Ilican et al. demonstrated that ZnO thin films formed using a sol with a pH value of 7.0 exhibited good crystallinity [3]. Therefore, the pH value of each as-synthesized sol was adjusted to 7.0.

XRD patterns of the undoped and B-doped ZnO thin films are shown in Fig. 1. From comparison with the standard XRD pattern of ZnO crystal (JCPDS 036-1451), these polycrystalline ZnO-based thin films were confirmed to show the formation of a hexagonal wurtzite structure. That figure clearly displays that the full widths at half-maximum (FWHMs) for three major diffraction peaks, (100), (002), and (101), of the 1% B-doped thin film were more than twice as wide as that of the undoped thin film, and the FWHMs of the B-doped thin films continued to broaden as B doping concentration was increased from 1% to 5%. Scherrer's formula was used to calculate the crystallite sizes of the films. Calculated results showed that ZnO thin film doped with 1% B drastically reduced the average crystallite sizes from 34.5 to 15.5 nm (Fig. 2). This reduction is attributed to distortion of the crystal lattice after the boron dopant was incorporated into the ZnO crystal. The distortion was caused by the large difference

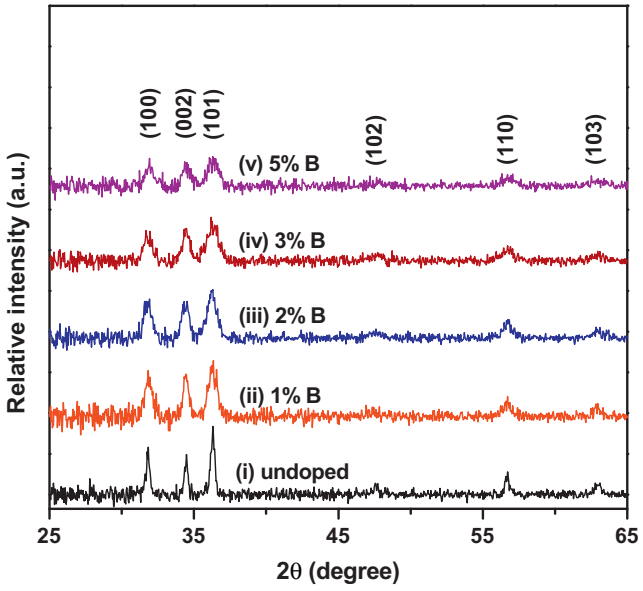

Fig. 1. XRD patterns of sol–gel derived undoped and B-doped ZnO thin films on glass substrates.

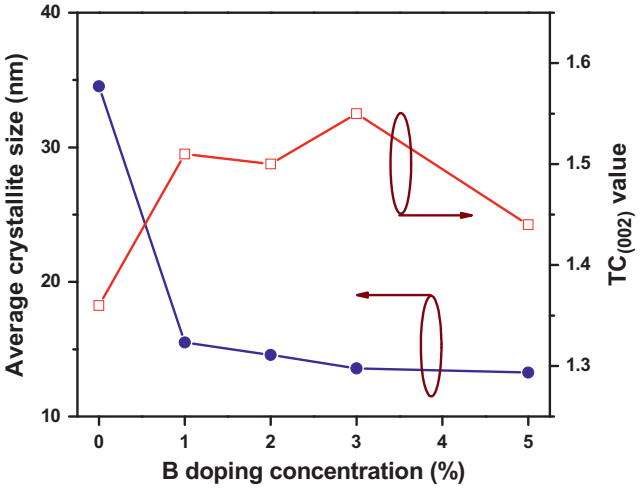

Fig. 2. Variation of average crystallite size and texture coefficient value in the (002) plane ($TC_{(002)}$) of ZnO:B thin films with B doping concentration.

between the ionic radii of B^{+3} (0.23 Å) and Zn^{+2} (0.74 Å) [24]. When the B doping concentration was increased from 1% to 5%, the average crystallite size of ZnO:B thin films decreased only slightly, from 14.6 to 13.3 nm (Fig. 2). The incorporation of greater amounts of B dopant into ZnO thin films not only caused lattice distortion but also tended to create lattice defects and nucleation centers [25]. Thus, the major mechanisms for the formation of fine grain microstructures in doped thin films are the increase of nucleation sites and limitation of grain growth.

The diffraction signals of the (102) and (103) planes of the 5% B-doped ZnO thin film were very weak (curve (v) in Fig. 1), which implies that the high B doping level caused the degree of crystallinity to degenerate. Kim et al. reported that with increasing B content in the ZnO crystal structure, the crystal symmetry can be broken, according to Raman spectra of ZnO:B thin films [24]. Moreover, it can also be seen that with increase in the B doping concentration, the diffraction intensity of the (002) plane gradually approached that of the (101) plane. Yamamoto et al. [26] and Pawar et al. [27] demonstrated that the crystal orientation of ZnO films was influenced by B doping concentration. The texture of the particular plane can be understood from the texture coefficient of the (*hkl*) plane ($TC_{(hkl)}$). This coefficient was calculated from data of XRD examination using the following formula [23]:

$$TC_{(hkl)} = \left(\frac{I_{(hkl)}/I_{r(hkl)}}{[1/n\sum I_{(hkl)}/I_{r(hkl)}]}\right) \quad (1)$$

where $I_{(hkl)}$ is the relative diffraction intensity of a plane (*hkl*) obtained from the film, *n* is the number of diffraction peaks considered, and $I_{r(hkl)}$ is the intensity of the plane (*hkl*) taken from the reference XRD data (JCPDS 036-1451). The values of $TC_{(002)}$ and $TC_{(101)}$ for the undoped ZnO thin film were 1.36 and 1.02, respectively. In B-doped ZnO thin films, the value of $TC_{(002)}$ increased (Fig. 2), while the value of $TC_{(101)}$ tended to decrease (e.g. $TC_{(002)}=1.51$ and $TC_{(101)}=0.88$ for 1% B-doped sample). That tendency is similar to previous reports that the (002) plane of ZnO crystal has the lowest surface energy [26,27].

Cross-sectional FE-SEM micrographs of the undoped and B-doped ZnO thin films are shown in Fig. 3. SEM images show that those ZnO-based polycrystalline thin films had an observably granular morphology; the B-doped thin films consisted of finer particles and exhibited a flatter surface than the undoped thin films did. The mean film thicknesses of the undoped and B-doped ZnO thin films were about 80 and 95 nm, depending on the viscosity of the coating solution and the parameters of the spin coating procedure. Moreover, our previous study reported that the surface of the undoped ZnO thin film showed irregular fiber-like stripes and a wrinkle network, presented by a low-magnification SEM image (10k ×) [28]. Caglar et al. reported a similar result; such features were observed from an AFM image [5]. However, the surface of the undoped ZnO thin film did not display such features in the present study because the sol stabilizer used was diethanolamine (DEA) instead of the typical monoethanolamine (MEA).

Each inserted image in the cross-sectional SEM photographs is a plane view SEM micrograph (high-magnification of 100k ×) of the corresponding thin film sample. The incorporation of boron dopant into ZnO thin films remarkably reduced the particle size and shrank the pores size. Both plane view and cross-sectional SEM images showed that some pores formed inside the sol–gel derived ZnO-based thin films; this formation was attributed to the decomposition of residual organics in dried sol–gel films. That decomposition is one of the major reasons why the quality of solution-processed oxide films is lower than that of sputtered oxide films.

Fig. 4 shows SPM images of the undoped and B-doped thin films. The images show the significant particle configuration,

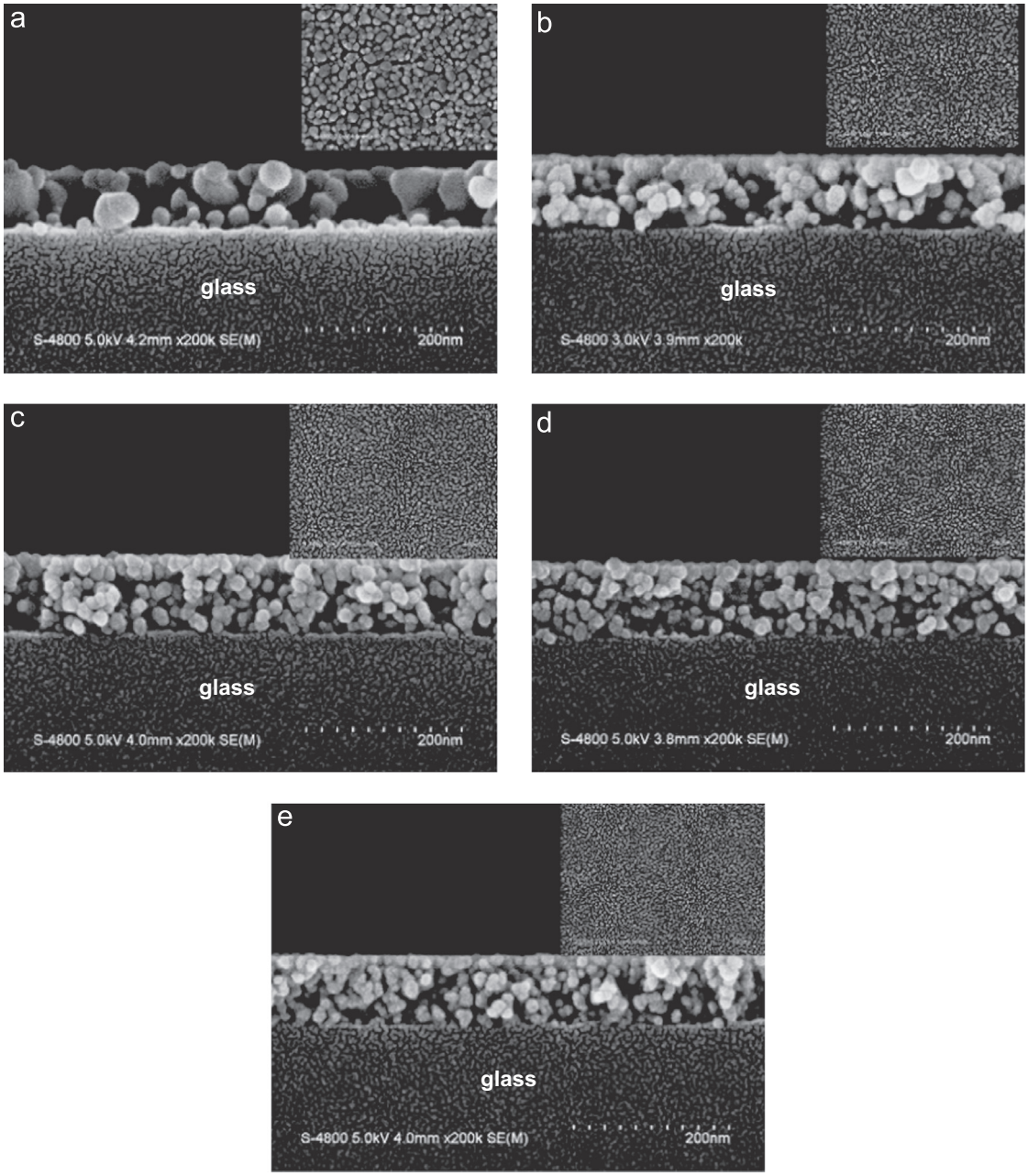

Fig. 3. Cross-sectional FE-SEM micrographs of B-doped ZnO thin films: (a) undoped, (b) 1%, (c) 2%, (d) 3%, and (e) 5% B-doped thin films.

and that the average particle size of the undoped thin film was larger than that of B-doped thin films. In addition, B-doped thin film samples exhibited flat, dense surfaces, because their finer particles increased the packing density and reduced the surface roughness. The surface conditions of polycrystalline oxide thin films are strongly related to their microstructures, especially particle size. Fig. 5 shows that the value of the surface root mean square (RMS) roughness was significantly reduced from 4.43 nm to 2.42 nm when 1% B was doped in ZnO. When the B doping level was higher than 1%, the value of RMS roughness decreased nearly linearly to 1.48 nm at a B doping concentration of 5%. Such a tendency is consistent with the results of XRD measurements and SEM observations.

3.2. Study of electrical transport and optical properties of ZnO:B thin films

Hall effect measurements were used to examine the electrical properties of ZnO thin films with different B doping concentrations, and the results are shown in Fig. 6. The 1% B-doped ZnO thin film exhibited the best electrical properties: Hall mobility (μ) of 17.9 $cm^2/V\,s$, electron concentration (n) of $1.2 \times 10^{15}\,cm^{-3}$, and resistivity ($\rho$) of $2.2 \times 10^2\,\Omega\,cm$. The initial increase in electrical properties with B doping concentration, especially electron concentration, is attributed to the incorporation of boron into ZnO thin films. The substitution of B^{3+} in a Zn^{2+} site as a donor can provide one charge carrier for conduction

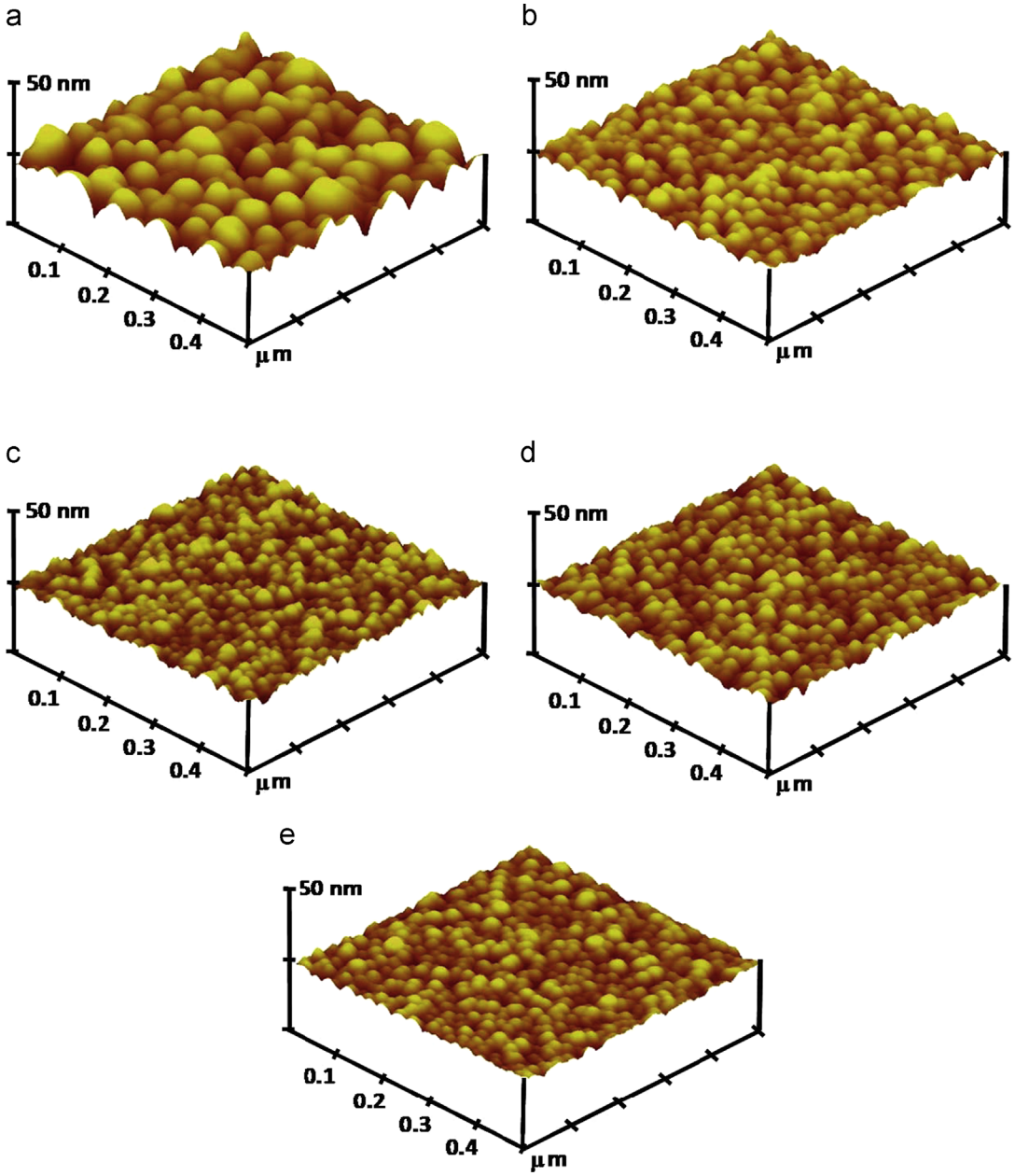

Fig. 4. SPM images of the surface of B-doped ZnO thin films: (a) undoped, (b) 1%, (c) 2%, (d) 3%, and (e) 5% B-doped thin films.

between the ZnO lattices [29]. Furthermore, the Hall mobility and electron concentration decreased as the B doping concentration increased from 1% to 5%. In addition, the trend of variation of resistivity with B doping concentration is the opposite of electron concentration because n-type semiconductor materials generally have an inverse relationship between resistivity and electron concentration ($\rho \propto 1/n$).

The decrease in electron concentration for ZnO thin films doped with boron concentrations higher than 1% can be explained. These nanostructured thin films possessed a greater number of grain boundaries to trap electrons, and excess B doping concentrations would form neutral defects (such as clusters and precipitates) rather than generating carriers [24,27]. In a polycrystalline conducting oxide and oxide semiconductor thin film, grain boundary scattering is an important mechanism if the grain size is small [30]. The grain boundaries form a potential barrier and trap or limit the mobility of charges, thereby decreasing the conductivity of the films [16,31]. The decrease in Hall mobility is considered to increase the number of scattering centers (creating a number of neutral defects) and create a potential barrier (increasing grain boundary density) when the ZnO thin films are doped with a high level of B dopant.

The optical properties of ZnO:B thin films were studied by measuring the transmittance across the full UV–vis range of 200–800 nm. Fig. 7 shows the optical transmittance spectra of glass/ZnO:B thin film samples. These transmittance spectra exhibited a strong absorption behavior in the UV region. The first derivative ($dT/d\lambda$) of optical transmittance in the

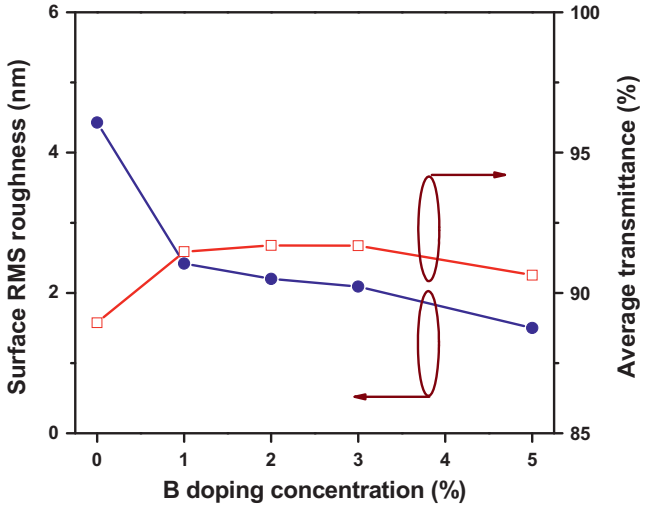

Fig. 5. Variation of surface RMS roughness and average transmittance in the visible region of ZnO:B thin films with B doping concentration.

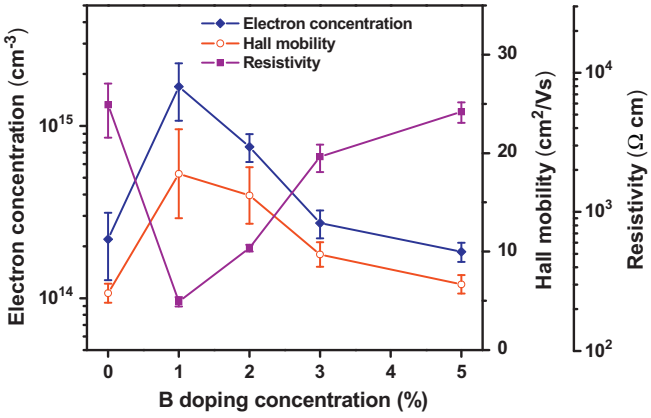

Fig. 6. Dependence of electrical properties (electron concentration, Hall mobility, and resistivity) of ZnO:B thin films as a function of B doping concentration.

wavelength range of 325–475 nm of the undoped and B-doped ZnO thin films was calculated to determine the absorption edge of these thin films. The inset of Fig. 7 shows the plot of $dT/d\lambda$ vs. wavelength, where a peak corresponds to the absorption edge. The absorption wavelength values of the undoped, 1%, 2%, 3%, and 5% B-doped ZnO thin films were 375, 373, 372, 371, and 370 nm, respectively. The wavelength of the absorption edge showed a blue shift.

The average transmittance values of ZnO:B thin films were calculated for wavelengths of 400–750 nm. Calculated results showed that the average transmittances (T_{ave}) of the undoped, 1%, 2%, 3%, and 5% B-doped ZnO thin films were 88.9%, 91.5%, 91.7%, and 90.6%, respectively. The B-doped thin films showed a higher average transmittance than the undoped thin film in the visible range, may due to such films exhibit the flat surface and the low porosity. The optical band gap of semiconductor thin films can be analyzed from the absorption properties. The absorption

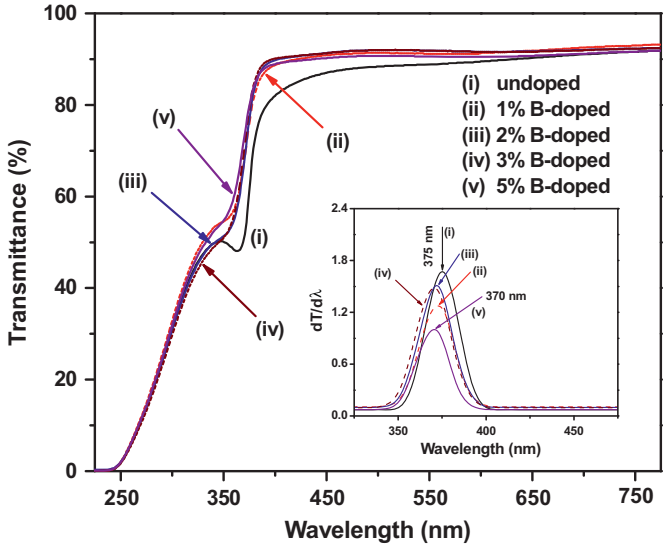

Fig. 7. Optical transmittance spectra of the undoped and B-doped ZnO thin films on glass substrates. The inset is the plot of $dT/d\lambda$ vs. wavelength of the undoped and B-doped ZnO thin films.

coefficient (α) and optical band gap (E_g) are related by the following equation [24,32]:

$$(\alpha h\nu) = B(h\nu - E_g)^n \quad (2)$$

where $h\nu$ is the photon energy, and B is an energy-independent constant. The nature of the transition is represented by the power factor n. For a direct transition, the value of factor n is 1/2. The absorption coefficient (α) can be obtained through Lambert's law from the transmittance data, which is expressed by the following relation:

$$\alpha = \frac{1}{t}\ln(T) \quad (3)$$

where t is the film thickness and T is the transmittance of film. Fig. 8(a) shows that the optical band gap of each ZnO-based semiconductor thin film was determined by extrapolating the linear portion of the curve from the plot of $(\alpha h\nu)^2$ vs. $h\nu$ and intercepting the x-axis at $(\alpha h\nu)^2$ equals to 0. The E_g values of the undoped, 1%, 2%, 3%, and 5% B-doped ZnO thin films were 3.25, 3.28, 3.29, 3.30, and 3.30 eV, respectively. Houng et al. reported that the values of the optical band gap changed with different crystalline structures in ZnO:B thin films due to grain size effect [4]. Not only the change in grain size but also the increase in the carrier density caused the broadening of the energy band, leading to blue shift in the optical band gap [23].

The width of the tail of the localized states in the band gap resulted from the structural disorder and defects of the semiconductor thin films. These in turn affected their optical band gap structure and optical transitions, which can be characterized by the slope of the Urbach tail or Urbach energy [33]. The absorption coefficient (α) near the band edge is an exponential dependence on photon energy,

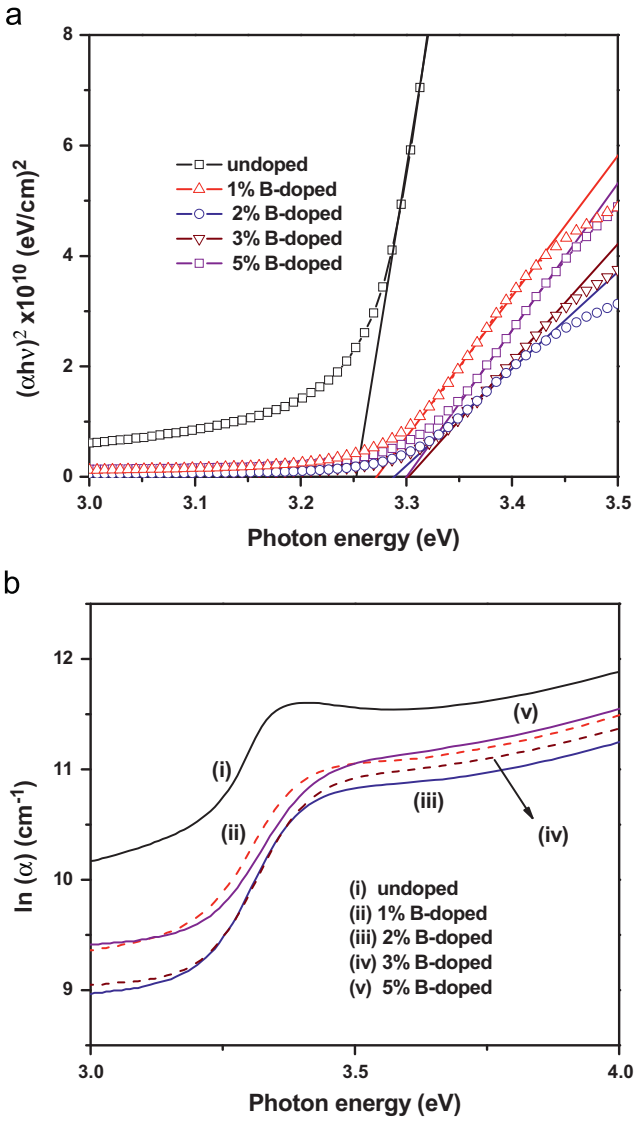

Fig. 8. Plots of (a) $(\alpha h\nu)^2$ vs. $h\nu$ and (b) $\ln(\alpha)$ vs. $h\nu$ for the undoped and B-doped ZnO thin films.

$h\nu$, as expressed by the following equation [33,34]:

$$\alpha = \alpha_0 \exp\left(\frac{h\nu}{E_U}\right), \quad (4)$$

where α_0 is a constant and E_U is the Urbach energy. The Urbach energy (E_U) was determined from the plot of $\ln(\alpha)$ vs. $h\nu$ (Fig. 8(b)), where the E_U values could be obtained from the reciprocal gradient of the linear potion of the plot [34]. The E_U values of the undoped, 1%, 2%, 3%, and 5% ZnO thin films were 102.7, 111.1, 111.6, 118.5, and 138.5 meV, respectively. Calculations showed that the Urbach energies of B-doped thin films were higher than that of the undoped thin film. The increase in the E_U value indicated that the structural disorder and defects in ZnO:B thin films increased with B doping concentration.

4. Conclusions

Boron-doped zinc oxide (ZnO:B) transparent semiconductor thin films were deposited onto alkali-free glasses by the sol–gel method and the spin coating technique. The ZnO thin films doped with B showed a remarkable modification in microstructure and surface condition. All ZnO:B thin films exhibited high optical transmittance ($T_{ave} > 90.5\%$) in the visible region. The optical band gap of the B-doped ZnO thin films slightly shifted to higher energy than that of the undoped ZnO thin film. Moreover, the increase in the Urbach energy of ZnO:B thin films suggested that the structural disorder and defects increased with B doping concentration. Polycrystalline ZnO-based thin films with the highest Hall mobility of 17.9 $cm^2/V\,s$ and the lowest electrical resistivity of $2.2 \times 10^2\ \Omega\,cm$ were obtained at the optimal boron doping concentration of 1%. Such as-prepared transparent oxide semiconductor thin films could be used as the active layer in functional transparent electronics.

Acknowledgments

This study received financial support from the National Science Council of the Republic of China (ROC) under Contract number NSC 99-2221-E-035-034-MY3. The authors gratefully acknowledge the Precision Instrument Support Center of Feng Chia University in providing the measurement facilities.

References

[1] H.V. Wenckstern, H. Schmidt, M. Brandt, A. Lajn, R. Pickenhain, M. Lorenz, M. Grundmann, D.M. Hofmann, A. Polity, B.K. Meyer, H. Saal, M. Binnewies, A. Börger, K.D. Becker, V.A. Tikhomirov, K. Jug, Anionic and cationic substitution in ZnO, Progress in Solid State Chemistry 37 (2009) 153–172.
[2] D.P. Norton, Y.W. Heo, M.P. Ivill, K. Ip, S.J. Pearton, M.F. Chisholm, T. Steiner, ZnO: growth, doping and processing, Materials Today 7 (2004) 34–40.
[3] S. Ilican, F. Yakuphanoglu, M. Caglar, Y. Caglar, The role of pH and boron doping on the characteristics of sol gel derived ZnO films, Journal of Alloys and Compounds 509 (2011) 5290–5294.
[4] B. Houng, C.L. Huang, S.Y. Tsai, Effect of the pH on the growth and properties of sol–gel derived boron-doped ZnO transparent conducting thin film, Journal of Crystal Growth 307 (2007) 328–333.
[5] M. Caglar, S. Ilican, Y. Caglar, F. Yakuphanoglu, Boron doped nanostructure ZnO films onto ITO substrate, Journal of Alloys and Compounds 509 (2011) 3177–3182.
[6] M.D. McCluskey, S.J. Jokela, Defects in ZnO, Journal of Applied Physics 106 (2009) 071101.
[7] J.H. Lee, B.O. Park, Transparent conducting ZnO:Al, In and Sn thin films deposited by the sol–gel method, Thin Solid Films 426 (2003) 94–99.
[8] C.Y. Tsay, W.C. Lee, Effect of dopants on the structural, optical and electrical properties of sol–gel derived ZnO semiconductor thin films, Current Applied Physics 13 (2013) 60–65.
[9] R.B.H. Tahar, N.B.H. Tahar, Boron-doped zinc oxide thin films prepared by sol–gel technique, Journal of Materials Science 40 (2005) 5285–5289.
[10] S. Jana, A.S. Vuk, A. Mallick, B. Orel, P.K. Biswas, Effect of boron doping on optical properties of sol–gel based nanostructured zinc

oxide films on glass, Materials Research Bulletin 46 (2011) 2392–2397.
[11] X.L. Chen, B.H. Xu, J.M. Xue, Y. Zhao, C.C. Wei, J. Sun, Y. Wang, X.D. Zhang, X.H. Geng, Boron-doped zinc oxide thin films for large-area solar cells grown by metal organic chemical vapor deposition, Thin Solid Films 515 (2007) 3753–3759.
[12] J. Steinhauser, S. Faÿ, N. Oliveira, E.V. Sauvain, D. Zimin, U. Kroll, C. Ballif, Electrical transport in boron-doped polycrystalline zinc oxide thin films, Physica Status Solidi A 205 (2008) 1983–1987.
[13] A. Shah, J. Meier, A. Buechel, U. Kroll, J. Steinhauser, F. Meillaud, H. Schade, D. Dominé, Towards very low-cost mass production of thin-film silicon photovoltaic (PV) solar modules on glass, Thin Solid Films 502 (2006) 292–299.
[14] S. Faÿ, J. Steinhauser, N. Oliveira, E.V. Sauvain, C. Ballif, Opto-electronic properties of rough LP-CVD ZnO:B for use as TCO in thin-film silicon solar cells, Thin Solid Films 515 (2007) 8558–8561.
[15] S. Faÿ, J. Steinhauser, S. Nicolay, C. Ballif, Polycrystalline ZnO: B grown by LPCVD as TCO for thin film silicon solar cells, Thin Solid Films 518 (2010) 2961–2966.
[16] A. Favier, D. Muñoz, S.M. de Nicolás, P.J. Ribeyron, Boron-doped zinc oxide layers grown by metal–organic CVD for silicon hetero-junction solar cells applications, Solar Energy Materials and Solar Cells 95 (2011) 1057–1061.
[17] N.M. Muhammad, N. Duraisamy, K. Rahman, H.W. Dang, J. Jo, K.H. Choi, Fabrication of printed memory device having zinc-oxide active nano-layer and investigation of resistive switching, Current Applied Physics 13 (2013) 90–96.
[18] S.T. Meyers, J.T. Anderson, C.M. Hung, J. Thompson, J.F. Wager, D.A. Keszler, Aqueous inorganic inks for low-temperature fabrication of ZnO TFTs, Journal of the American Chemical Society 130 (2008) 17603–17609.
[19] C.T. Liu, W.H. Lee, T.L. Shih, Synthesis of ZnO nanoparticles to fabricate a mask- free thin-film transistor by inkjet printing, Journal of Nanotechnology 2012 (2012) 710908.
[20] W.J. Park, H.S. Shin, B.D. Ahn, G.H. Kim, S.M. Lee, K.H. Kim, H.J. Kim, Investigation on doping dependency of solution-processed Ga-doped ZnO thin film transistor, Applied Physics Letters 93 (2008) 083508.
[21] S.Y. Park, B.J. Kim, K. Kim, M.S. Kang, K.H. Lim, T.I. Lee, J.M. Myoung, H.K. Baik, J.H. Cho, Y.S. Kim, Low-temperature, solution-processed and alkali metal doped ZnO for high-performance thin-film transistors, Advanced Materials 24 (2012) 834–838.
[22] B.Y. Su, S.Y. Chu, Y.D. Juang, Improved electrical and thermal stability of solution-processed Li-doped ZnO thin-film transistors, IEEE Transactions on Electron Devices 59 (2012) 700–704.
[23] C.Y. Tsay, K.S. Fan, C.M. Lei, Synthesis and characterization of sol–gel derived gallium-doped zinc oxide thin films, Journal of Alloys and Compounds 512 (2012) 216–222.
[24] G. Kim, J. Bang, Y. Kim, S.K. Rout, S.I. Woo, Structural, electrical and optical properties of boron doped ZnO thin films using LSMCD method at room temperature, Applied Physics A 97 (2009) 821–828.
[25] J. Hu, R.G. Gordon, Atmospheric pressure chemical vapor deposition of gallium doped zinc oxide thin films from diethyl zinc, water, and triethyl gallium, Journal of Applied Physics 72 (1992) 5381–5392.
[26] Y. Yamamoto, K. Saito, K. Takahashi, M. Konagai, Preparation of boron-doped ZnO thin films by photo-atomic layer deposition, Solar Energy Materials and Solar Cells 65 (2001) 125–132.
[27] B.N. Pawar, S.R. Jadkar, M.G. Takwale, Deposition and characterization of transparent and conductive sprayed ZnO:B thin films, Journal of Physics and Chemistry of Solids 66 (2005) 1779–1782.
[28] C.Y. Tsay, C.W. Wu, C.M. Lei, F.S. Chen, C.K. Lin, Microstructural and optical properties of Ga-doped ZnO semiconductor thin films prepared by sol–gel process, Thin Solid Films 519 (2010) 1516–1520.
[29] K. Ellmer, Resistivity of polycrystalline zinc oxide films: current status and physical limit, Journal of Physics D: Applied Physics 34 (2001) 3097–3108.
[30] A.K. Kulkarni, K.H. Schulz, T.S. Lim, M. Khan, Dependence of the sheet resistance of indium-tin-oxide thin films on grain size and grain orientation determined from X-ray diffraction techniques, Thin Solid Films 345 (1999) 273–277.
[31] J. Steinhauser, S. Faÿ, N. Oliveira, E.V. Sauvain, C. Ballif, Transition between grain boundary and intragrain scattering transport mechanisms in boron-doped zinc oxide thin films, Applied Physics Letters 90 (2007) 142107.
[32] J. Tauc, R. Grigorovici, A. Vancu, Optical properties and electronic structure of amorphous germanium, Physica Status Solidi B 15 (1966) 627–637.
[33] S. Aksoy, Y. Caglar, S. Ilican, M. Caglar, Sol–gel derived Li–Mg co-doped ZnO films: preparation and characterization via XRD, XPS, FESEM, Journal of Alloys and Compounds 512 (2012) 171–178.
[34] M.H. Mamat, M.Z. Sahdan, S. Amizam, H.A. Rafaie, Z. Khusaimi, M. Rusop, Optical and electrical properties of aluminum doped zinc oxide thin films at various doping concentrations, Journal of the Ceramic Society of Japan 117 (2009) 1263–1267.